Journal of Zhejiang University-SCIENCE B (Biomedicine & Biotechnology) *2024 25(5):422-437*
www.jzus.zju.edu.cn; www.springer.com/journal/11585
E-mail: jzus_b@zju.edu.cn

Research Article

https://doi.org/10.1631/jzus.B2300077

Check for updates

Exosomal *let-7a-5p* derived from human umbilical cord mesenchymal stem cells alleviates coxsackievirus B3-induced cardiomyocyte ferroptosis via the SMAD2/ZFP36 signal axis

Xin LI[1,2,3,4,5], Yanan HU[6], Yueting WU[1,2,3,4,5], Zuocheng YANG[6], Yang LIU[1,2,3,4,5]✉, Hanmin LIU[1,2,3,4,5]✉

[1]*Department of Pediatric Pulmonology and Immunology, West China Second University Hospital, Sichuan University, Chengdu 610041, China*
[2]*Key Laboratory of Birth Defects and Related Diseases of Women and Children (Sichuan University), Ministry of Education, Chengdu 610041, China*
[3]*NHC Key Laboratory of Chronobiology (Sichuan University), Chengdu 610041, China*
[4]*The Joint Laboratory for Lung Development and Related Diseases of West China Second University Hospital, Sichuan University and School of Life Sciences of Fudan University, West China Institute of Women and Children's Health, West China Second University Hospital, Sichuan University, Chengdu 610041, China*
[5]*Sichuan Birth Defects Clinical Research Center, West China Second University Hospital, Sichuan University, Chengdu 610041, China*
[6]*Department of Pediatrics, the Third Xiangya Hospital, Central South University, Changsha 410013, China*

Abstract: Viral myocarditis (VMC) is one of the most common acquired heart diseases in children and teenagers. However, its pathogenesis is still unclear, and effective treatments are lacking. This study aimed to investigate the regulatory pathway by which exosomes alleviate ferroptosis in cardiomyocytes (CMCs) induced by coxsackievirus B3 (CVB3). CVB3 was utilized for inducing the VMC mouse model and cellular model. Cardiac echocardiography, left ventricular ejection fraction (LVEF), and left ventricular fractional shortening (LVFS) were implemented to assess the cardiac function. In CVB3-induced VMC mice, cardiac insufficiency was observed, as well as the altered levels of ferroptosis-related indicators (glutathione peroxidase 4 (GPX4), glutathione (GSH), and malondialdehyde (MDA)). However, exosomes derived from human umbilical cord mesenchymal stem cells (hucMSCs-exo) could restore the changes caused by CVB3 stimulation. *Let-7a-5p* was enriched in hucMSCs-exo, and the inhibitory effect of hucMSCs-exo$^{let\text{-}7a\text{-}5p\ mimic}$ on CVB3-induced ferroptosis was higher than that of hucMSCs-exo$^{mimic\ NC}$ (NC: negative control). Mothers against decapentaplegic homolog 2 (SMAD2) increased in the VMC group, while the expression of zinc-finger protein 36 (ZFP36) decreased. *Let-7a-5p* was confirmed to interact with *SMAD2* messenger RNA (mRNA), and the SMAD2 protein interacted directly with the ZFP36 protein. Silencing *SMAD2* and overexpressing *ZFP36* inhibited the expression of ferroptosis-related indicators. Meanwhile, the levels of GPX4, solute carrier family 7, member 11 (SLC7A11), and GSH were lower in the *SMAD2* overexpression plasmid (oe-*SMAD2*)+*let-7a-5p* mimic group than in the oe-NC+*let-7a-5p* mimic group, while those of MDA, reactive oxygen species (ROS), and Fe^{2+} increased. In conclusion, these data showed that ferroptosis could be regulated by mediating *SMAD2* expression. Exo-*let-7a-5p* derived from hucMSCs could mediate *SMAD2* to promote the expression of ZFP36, which further inhibited the ferroptosis of CMCs to alleviate CVB3-induced VMC.

Key words: Exosome; *Let-7a-5p*; Mothers against decapentaplegic homolog 2 (SMAD2); Coxsackievirus B3 (CVB3); Ferroptosis

1 Introduction

Viral myocarditis (VMC) is one of the predominant causes of dilated cardiomyopathy and sudden cardiac death (Huber, 2016). VMC can elicit severe heart diseases, such as acute heart failure, ventricular arrhythmias, and cardiogenic shock in the clinic (Inamdar and Inamdar, 2016). Therefore, it is urgent to establish an effective intervention program to alleviate VMC.

Ferroptosis is considered to be actively involved in the regulation of cell death in cardiomyocytes (CMCs) (Rodríguez-Graciani et al., 2022). However, the relationship between ferroptosis and VMC has not been clearly defined. Our previous studies have demonstrated

✉ Yang LIU, cyggly@126.com
Hanmin LIU, liuhm@scu.edu.cn
Yang LIU, https://orcid.org/0000-0003-4626-3618
Hanmin LIU, https://orcid.org/0000-0002-4633-911X

Received Feb. 7, 2023; Revision accepted June 29, 2023; Crosschecked Apr. 22, 2024

that the ferroptosis of CMCs could be induced by coxsackievirus B3 (CVB3), the most common and fetal causative agent of VMC. Meanwhile, the mothers against decapentaplegic homolog (SMAD) signal was found to be involved in the regulation of iron metabolism (Camaschella et al., 2020), and the SMAD signaling pathway was overactivated after CVB3 infection (Chen et al., 2011). Thus, we rationally focused on the SMAD signal and ferroptosis in CVB3-induced VMC.

Exosomes secreted by human umbilical cord mesenchymal stem cells (hucMSCs-exo) have shown therapeutic effects in a variety of diseases (Shao et al., 2020; Wang et al., 2020; Yuan et al., 2021). A recent study has found that hucMSCs-exo can alleviate VMC (Gu et al., 2020). Meanwhile, *let-7a-5p* can serve as a mediator of cell communication and a biomarker of cardiovascular diseases (Bao et al., 2013). Exosomal *let-7* family members were found to be effective in improving pulmonary fibrosis (Sun et al., 2019) and regulating proliferation, apoptosis, and pyroptosis through various signaling pathways (Chen et al., 2019). Furthermore, *let-7a-5p* was associated with SMAD2 in tumor inhibition and the regulation of cell processes (Xia et al., 2021). Even though it is a fascinating topic to investigate whether exosomal *let-7a-5p* from hucMSCs plays a role in mediating the SMAD signal during the progression of VMC, no definitive answer has been given.

Therefore, we constructed VMC mouse and cell models using CVB3. To study the effect of exo-*let-7a-5p* from hucMSCs on ferroptosis in CVB3-induced VMC and the role of the *let-7a-5p*/SMAD2 signaling axis in this regulatory pathway (Fig. S1), the levels of ferroptosis-related markers were analyzed by regulating *let-7a-5p*, SMAD2, and zinc-finger protein 36 (ZFP36) via exosomes. Our in-depth investigation helps to clarify the therapeutic mechanism of hucMSCs-exo in VMC, which is expected to become a new effective treatment alternative.

2 Materials and methods

2.1 Isolation and culture of hucMSCs

HucMSCs were isolated from a fresh umbilical cord of an informed consenting mother, according to a previously described protocol (Qiao et al., 2008). The umbilical cord was initially washed with Dulbecco's modified Eagle's medium (DMEM; Sigma, St. Louis, USA) to remove the residual blood before chopping it into small pieces (about 3 mm), which were incubated in DMEM culture medium at 37 °C. After the degree of fusion reached 80%, hucMSCs were treated with trypsin and then cultured. HucMSCs from the third to fifth generations were used for further experiments.

Inhibitor negative control (NC), *let-7a-5p* inhibitor, mimics NC, and *let-7a-5p* mimics were purchased from GenePharma (Shanghai, China). The hucMSCs were transfected with inhibitor NC, *let-7a-5p* inhibitor, mimics NC, and *let-7a-5p* mimics with lipofectamine 2000 for 48 h. Exosome extraction was performed after reaching 80% cell confluence. The exosome extraction and identification protocols were described in supplementary materials and methods.

2.2 Animals and treatment

BALB/c mice were provided by Hunan SJA Laboratory Animal Co., Ltd. (Hunan, China). The in vivo VMC mouse model was created using CVB3 (ATCC, Manassas, VA, USA). The 50% tissue culture infective dose ($TCID_{50}$) was determined to measure the viral titers in HeLa cells before infection.

Experiment 1: BALB/c mice were randomly divided into two groups, including normal and VMC groups. Mice in the VMC group received an intraperitoneal injection of 0.1 mL of 1×10^3 $TCID_{50}$ CVB3 in phosphate-buffered saline (PBS), and an equal volume of PBS was intraperitoneally injected as the control (normal). After 7 d, the mice were euthanized after echocardiography and the determination of cardiac function parameters (Li JH et al., 2021), followed by the collection of myocardial tissue.

Experiment 2: The mice were randomly divided into seven groups, including normal, VMC, husMSCs-exo, hucMSCs-exo$^{\text{inhibitor NC}}$, hucMSCs-exo$^{\textit{let-7a-5p}\text{ inhibitor}}$, hucMSCs-exo$^{\text{mimic NC}}$, and hucMSCs-exo$^{\textit{let-7a-5p}\text{ mimic}}$ groups. Mice in the normal and VMC groups were treated as described previously. The animals were injected with 0.1 mL CVB3 24 h later, and then husMSCs-exo, hucMSCs-exo$^{\text{inhibitor NC}}$, hucMSCs-exo$^{\textit{let-7a-5p}\text{ inhibitor}}$, hucMSCs-exo$^{\text{mimic NC}}$, and hucMSCs-exo$^{\textit{let-7a-5p}\text{ mimic}}$ (50 μg/mouse) were injected intravenously into each group as a previous report (Gu et al., 2020). After 7 d, all mice were euthanized after echocardiography. Subsequently, mouse myocardial tissue was collected for experimental analysis.

2.3 Cell culture experiment

The primary CMCs were isolated from neonatal BALB/c mice, and CVB3 was maintained by HeLa cells as previously described (Li J et al., 2021). HeLa cells and CMCs were cultured in DMEM. The $TCID_{50}$ assay was performed in HeLa cells.

Experiment 1: CMCs were grouped as follows: normal, control, control+ferrostain-1, ferrostain-1, and erastin groups. CMCs were cultured with CVB3-infected HeLa cells in the control group and received no treatment in the normal group. CMCs in the ferrostain-1 group were treated with 10 μmol/L ferrostain-1 (A4371, APExBIO, USA), CMCs in the control+ferrostain-1 group were treated with CVB3 and 10 μmol/L ferrostain-1, and 40 μmol/L erastin (B1524, APExBIO, USA) was used to treat CMCs in the erastin group.

Experiment 2: CMCs were grouped as follows: normal, control, and hucMSCs-exo groups. CMCs were cultured with CVB3-infected HeLa cells in the control group and received no treatment in the normal group. CMCs in the hucMSCs-exo group were cultured with CVB3-infected HeLa cells and 50 μg/mL hucMSCs-exo for 24 h.

Experiment 3: CMCs were grouped as follows: normal, control, hucMSCs-exo, hucMSCs-exo$^{\text{mimic NC}}$, and hucMSCs-exo$^{\textit{let-7a-5p}\text{ mimic}}$ groups. Cells in the hucMSCs-exo$^{\text{mimic NC}}$ and hucMSCs-exo$^{\textit{let-7a-5p}\text{ mimic}}$ groups were cultured with CVB3-infected HeLa cells and 50 μg/mL hucMSCs-exo$^{\text{mimic NC}}$ and hucMSCs-exo$^{\textit{let-7a-5p}\text{ mimc}}$ exosomes, respectively. Cells in the normal, control, and hucMSCs-exo groups were treated as described previously.

Experiment 4: CMCs were grouped as follows: control, mimic NC, and *let-7a-5p* mimic groups. Cells in the mimic NC and *let-7a-5p* mimic groups were transfected with mimics NC and *let-7a-5p* mimics, respectively, and cultured with CVB3-infected HeLa cells. Cells in the control group were treated as described before.

Experiment 5: CMCs were grouped as follows: normal, control, NC overexpression plasmid (oe-NC)+mimic NC, oe-NC+*let-7a-5p* mimic, *SMAD2* overexpression plasmid (oe-*SMAD2*)+mimic NC, and oe-*SMAD2*+*let-7a-5p* mimic groups. CMCs were treated with CVB3 and transfected with different combinations of oe-*SMAD2*, *let-7a-5p* mimics, and their negative controls (oe-NC and mimic NC) in the oe-NC+mimic NC, oe-NC+*let-7a-5p* mimic, oe-*SMAD2*+mimic NC, and oe-*SMAD2*+*let-7a-5p* mimic groups. Cells in the normal and control groups were treated as described previously.

Experiment 6: CMCs were grouped as follows: control, ferrostain-1, ferrostain-1+small interfering RNA (siRNA)-NC (si-NC)+inhibitor NC, ferrostain-1+*let-7a-5p* inhibitor, ferrostain-1+siRNA-*SMAD2* (si-*SMAD2*), and ferrostain-1+si-*SMAD2*+*let-7a-5p* inhibitor groups. CMCs in the ferrostain-1 group were treated with CVB3 and ferrostain-1. In the ferrostain-1+si-NC+inhibitor NC, ferrostain-1+*let-7a-5p* inhibitor, ferrostain-1+si-*SMAD2*, and ferrostain-1+si-*SMAD2*+*let-7a-5p* inhibitor groups, CMCs were transfected with different combinations of si-*SMAD2*, *let-7a-5p* inhibitor, and their negative controls (si-NC and inhibitor NC) and were treated with CVB3 and ferrostain-1. Cells in the control group were treated as described previously.

Experiment 7: CMCs were grouped as follows: normal, control, si-NC+oe-NC, si-*SMAD2*+oe-NC, and si-*SMAD2*+oe-*ZFP36* groups. The different combinations of si-NC, si-*SMAD2*, oe-NC, and oe-*ZFP36* (GenePharma) were transfected into CVB3-treated CMCs in the si-NC+oe-NC, si-*SMAD2*+oe-NC, and si-*SMAD2*+oe-*ZFP36* groups. Cells in the normal and control groups were performed as described previously.

2.4 Statistical analysis

Statistics were carried out using GraphPad Prism 8.0.2 software (GraphPad Software, San Diego, USA). Data were presented as mean±standard deviation (SD) of three to nine independent experiments. A two-sided Student's *t*-test, one-way analysis of variance (ANOVA), and two-way ANOVA were performed to evaluate the difference between groups. Pearson correlation coefficient was performed to analyze the correlation between genes. *P* values of <0.05 were considered significant.

Further information was provided in the supplementary materials and methods.

3 Results

3.1 Identification of hucMSCs and exosomes

After the isolation of hucMSCs, their marker proteins (cluster of differentiation 44 (CD44), CD45, CD90, and CD105) were identified by flow cytometry (>98%; Figs. S2a and S2b). The osteogenic and adipogenic

differentiation potentials of hucMSCs were analyzed by Alizarin Red staining and Oil Red O staining, respectively (Figs. S2c and S2d). Next, exosomes were isolated from the hucMSC culture supernatants following the ultracentrifugation method and identified by nanoparticle tracking analysis (NTA), transmission electron microscopy (TEM), and western blot (Figs. S2e–S2g).

3.2 Ferroptosis of CMCs in CVB3-induced VMC

CVB3 was utilized to construct an in vivo VMC mouse model. Compared with the normal group, the myocardial tissues of the VMC model exhibited damaged structures under the electron microscope (Fig. 1a). The cardiac echocardiography demonstrated the compromised heart structure in VMC mice (Fig. 1b). Furthermore, the left ventricular ejection fraction (LVEF) and left ventricular fractional shortening (LVFS) were attenuated in the VMC group, as compared with the normal group (Fig. 1c). The LVEF in the VMC group was about half of that in the normal group, while the LVFS was even lower at only 40% of normal mice. Glutathione peroxidase 4 (GPX4) levels decreased in VMC mice (Fig. 1d). Glutathione (GSH) was lower in the VMC group than in the normal group, while malondialdehyde (MDA) showed the opposite trend (Figs. 1e and 1f).

Moreover, SMAD2 messenger RNA (mRNA) and protein levels were more actively expressed in the VMC group than in the normal group, while the ZFP36 expression was substantially suppressed. The two proteins demonstrated similar trends as the mRNA expression (Fig. 1g). SMAD2 maintained a high level, but ZFP36 was restrained at a low level. Based on the immunohistochemistry results, the expression of solute carrier family 7, member 11 (SLC7A11) in the myocardial tissues of VMC mice was attenuated, while protein 53 (p53) and prostaglandin G/H synthase 2 (PTGS2) increased, indicating ongoing ferroptosis (Fig. 1h). Based on these data, the ferroptosis of CMCs in VMC mice could be induced by CVB3 with high SMAD2 expression and low ZFP36 expression.

3.3 Effects of hucMSCs-exo on the CVB3-induced ferroptosis of CMCs and *let-7a-5p* levels

Next, to analyze the relationship between CVB3 and ferroptosis, we treated CMCs with CVB3, ferrostain-1, and erastin. Ferrostain-1 and erastin are inhibitors and activators of ferroptosis, respectively. The results of Calcein-AM/propidium iodide (PI) staining, reactive oxygen species (ROS) level, and protein expression (cyclooxygenase-2 (COX-2), Caspase-3, phosphorylated protein kinase B (p-AKT), and p-p70S6K) (Fig. S3) indicated that the effect of CVB3 intervention on CMCs was similar to that of erastin intervention. Meanwhile, ferrostain-1 could inhibit the effect of CVB3 on CMCs. Thus, it was speculated that CVB3 could induce ferroptosis in CMCs.

Subsequently, we established an in vitro model of CVB3 infection in CMCs and performed exosome treatment, which consisted of exosome uptake analysis, and the presence of green fluorescent signal in the cytoplasm indicated that cells had taken up the hucMSCs-exo (Fig. 2a). When infected by the virus, the proliferation of CMCs decreased and the apoptosis rate increased (Figs. 2b and 2c), which were reversed by the hucMSCs-exo intervention. The levels of GPX4, GSH, and SLC7A11 were higher in the hucMSCs-exo group than in the control group, while the expression levels of MDA, ROS, Fe^{2+}, p53, and PTGS2 decreased (Figs. 2d–2i). Meanwhile, the level of *let-7a-5p* was lower in the VMC group than in the normal group (Fig. 2j). After the hucMSCs-exo intervention, the expression of *let-7a-5p* increased (Fig. 2k). Further analysis showed that *let-7a-5p* was enriched in hucMSC-exo (Fig. 2l).

3.4 Effect of exo-*let-7a-5p* derived from hucMSCs on the ferroptosis of cardiac myocytes

As is known, profiting from their low immunogenicity and no self-replication, exosomes are qualified transporters to ensure cell-to-cell communication (Mathieu et al., 2019). *Let-7a-5p* can serve as a mediator of cell communication and biomarker of cardiovascular diseases (Bao et al., 2013). Furthermore, to detect whether the transfer of *let-7a-5p* in hucMSCs-exo plays an important role in the process, the model cells were treated with hucMSCs-exo, hucMSCs-exo$^{\text{mimic NC}}$, and hucMSCs-exo$^{\textit{let-7a-5p}\ \text{mimic}}$. The *let-7a-5p* levels were higher in the hucMSCs-exo$^{\textit{let-7a-5p}\ \text{mimic}}$ group than in the hucMSCs-exo$^{\text{mimic NC}}$ group (Fig. 3a). Proliferation was higher in the hucMSCs-exo$^{\textit{let-7a-5p}\ \text{mimic}}$ group compared to the hucMSCs-exo$^{\text{mimic NC}}$ group (Fig. 3b). At the same time, terminal deoxynucleotidyl transferase dUTP nick end labeling (TUNEL) assay was performed (Fig. 3c). The apoptosis rate decreased in the hucMSCs-exo$^{\textit{let-7a-5p}\ \text{mimic}}$ group compared with the hucMSCs-exo$^{\text{mimic NC}}$ group,

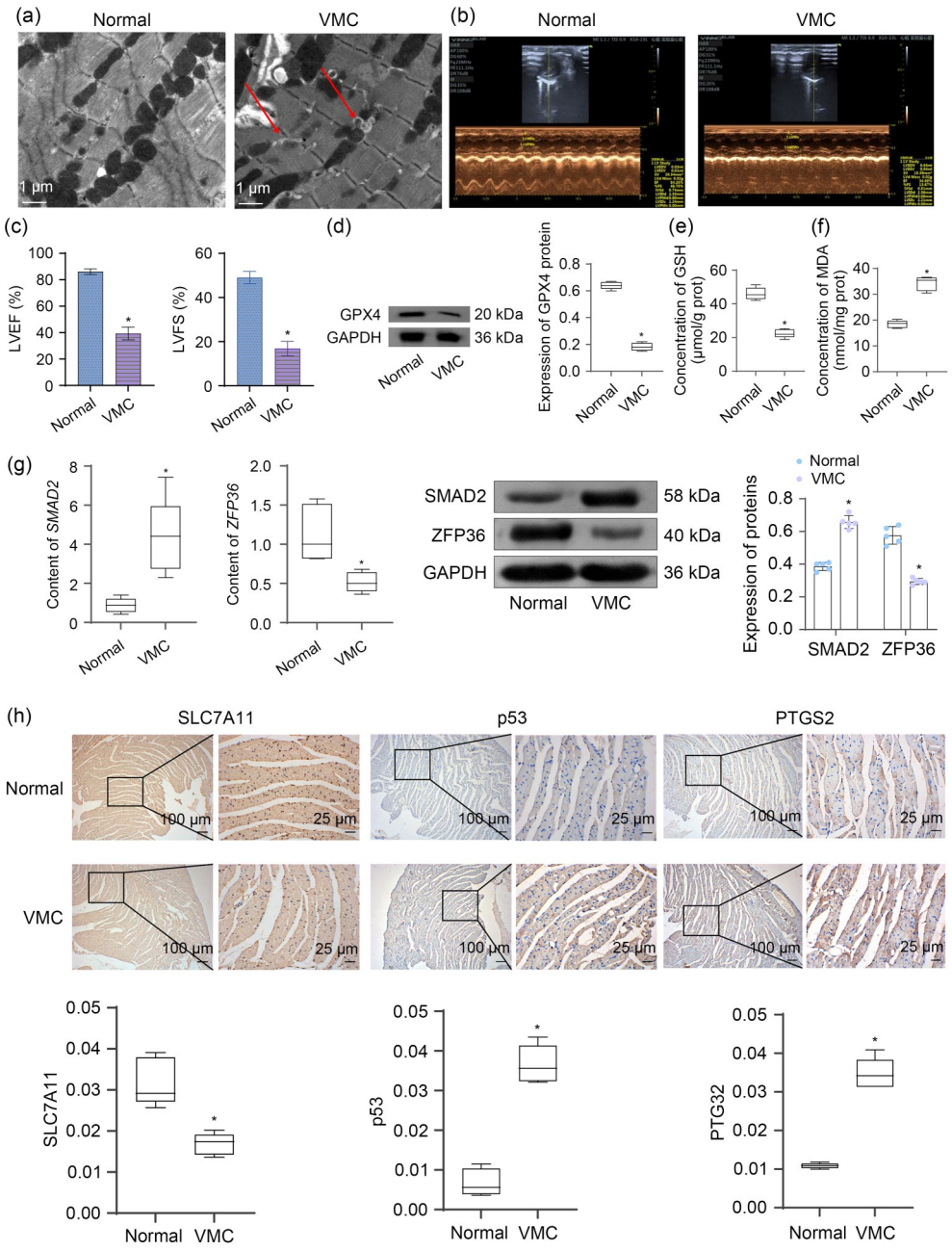

Fig. 1 Tissue damage and ferroptosis development in VMC mice. (a) TEM studies on the structure of isolated cardiac muscle from normal and VMC mice. Red arrows indicate damaged areas. (b) Ultrasound cardiograms of normal and VMC mice. (c) Comparison of LVEF and LVFS between normal and VMC mice. (d) GPX4 protein expression in myocardial tissue. (e, f) GSH and MDA levels in myocardial tissue. The two-sided Student's *t*-test was performed. (g) Expression of SMAD2 and ZFP36 in the VMC model. The two-sided Student's *t*-test and two-way ANOVA were performed to evaluate the difference. (h) Immunohistochemistry of SLC7A11, p53, and PTGS2 in the VMC model. The ratio of the cumulative optical density of positive expression site under the visual field to the sample area under the visual field was used to quantify the levels of SLC7A11, p53, and PTGS2. A two-sided Student's *t*-test was performed. Data were presented as mean±standard deviation (SD) of five independent experiments. *P<0.05 vs. normal. VMC: viral myocarditis; TEM: transmission electron microscopy; LVEF: left ventricular ejection fraction; LVFS: left ventricular fractional shortening; GPX4: glutathione peroxidase 4; GAPDH: glyceraldehyde-3-phosphate dehydrogenase; GSH: glutathione; MDA: malondialdehyde; SMAD2: mothers against decapentaplegic homolog 2; ZFP36: zinc-finger protein 36; SLC7A11: solute carrier family 7, member 11; p53: protein 53; PTGS2: prostaglandin G/H synthase 2; ANOVA: analysis of variance; prot: protein.

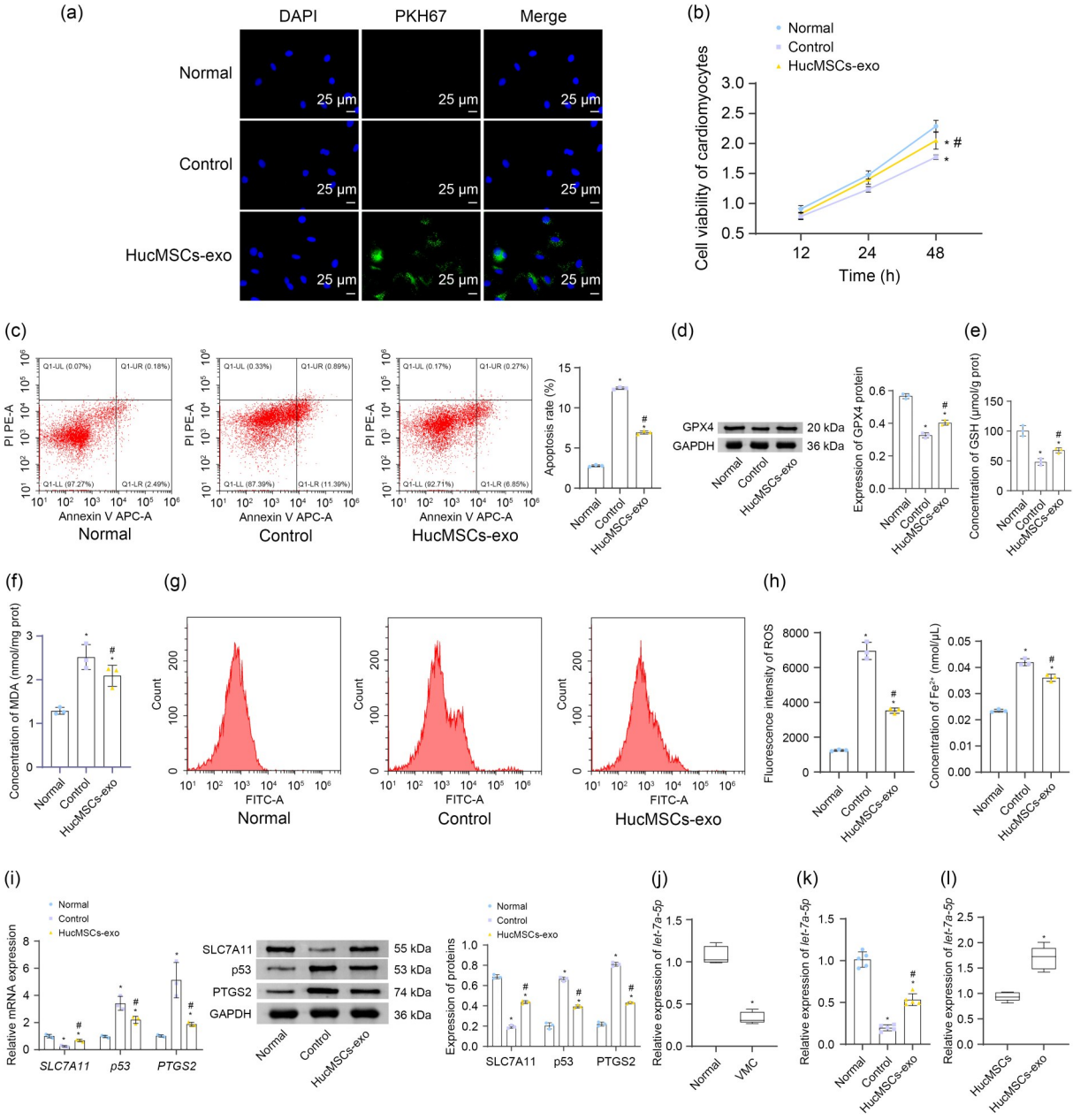

Fig. 2 Effects of hucMSCs-exo on the levels of *let-7a-5p* and the CVB3-induced ferroptosis of CMCs. (a) Cellular uptake of hucMSCs-exo analysis. (b) After hucMSCs-exo intervention, the proliferation of CMCs was measured at 12, 24, and 48 h. Two-way ANOVA was applied to evaluate the difference. (c) Apoptosis rate of CMCs. (d) Protein expression of GPX4. (e–h) Levels of GSH, MDA, ROS, and Fe^{2+}. One-way ANOVA was used to evaluate the difference. (i) The mRNA and protein levels of SLC7A11, PTGS2, and p53. Two-way ANOVA was used. (j) Expression of *let-7a-5p* between the normal and VMC groups. A two-sided Student's *t*-test was performed. (k) Quantification of *let-7a-5p* in the normal, control, and hucMSCs-exo groups. One-way ANOVA was used. (l) Quantification of *let-7a-5p* in the hucMSCs and hucMSCs-exo. A two-sided Student's *t*-test was applied. Data were presented as mean±standard deviation (SD) of three to five independent experiments. $^{*}P$<0.05 vs. normal or hucMSCs; $^{\#}P$<0.05 vs. control. HucMSCs-exo: exosomes secreted by human umbilical cord mesenchymal stem cells; CVB3: coxsackievirus B3; CMCs: cardiomyocytes; ANOVA: analysis of variance; GPX4: glutathione peroxidase 4; GSH: glutathione; MDA: malondialdehyde; ROS: reactive oxygen species; mRNA: messenger RNA; SLC7A11: solute carrier family 7, member 11; PTGS2: prostaglandin G/H synthase 2; p53: protein 53; VMC: viral myocarditis; GAPDH: glyceraldehyde-3-phosphate dehydrogenase; DAPI: 4',6-diamidino-2-phenylindole dihydrochloride; PI: propidium iodide; PE: phycoerythrin; APC: allophycocyanin; UL: upper left; UR: upper right; LL: lower left; LR: lower right; FITC: fluorescein isothiocyanate.

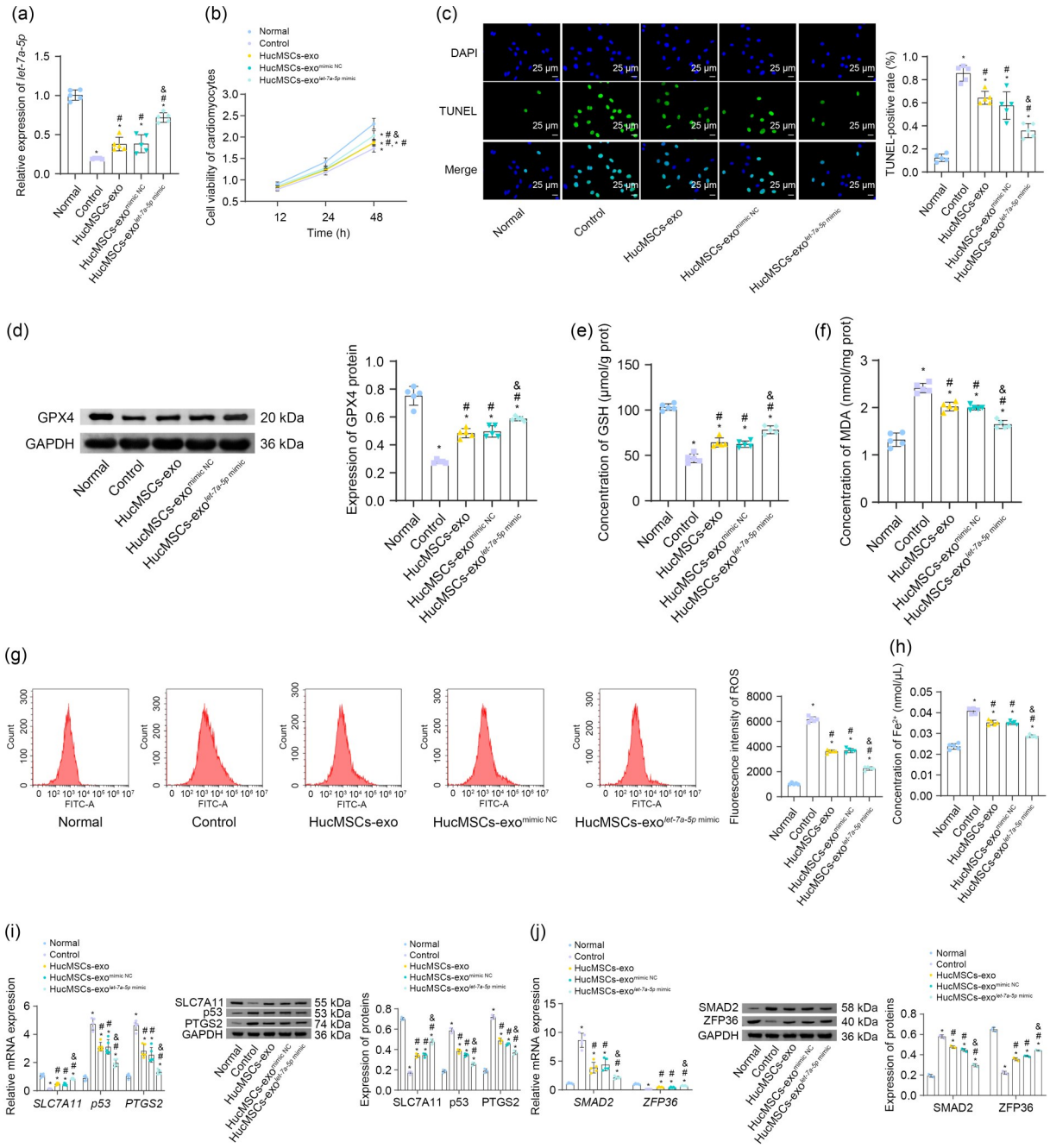

Fig. 3 Effect of exo-*let-7a-5p* on the ferroptosis of cardiac myocytes. (a) Expression of *let-7a-5p* in the normal, control, hucMSCs-exo, hucMSCs-exo$^{\text{mimic NC}}$, and hucMSCs-exo$^{\textit{let-7a-5p mimic}}$ groups. One-way ANOVA was performed. (b) Proliferation activity of CMCs in different treatment groups at 12, 24, and 48 h. Two-way ANOVA was performed. (c) The apoptotic rate of CMCs was revealed by TUNEL assay. (d) Expression of GXP4. (e–h) Levels of GSH, MDA, ROS, and Fe^{2+}. One-way ANOVA was performed. (i) Levels of SLC7A11, p53, and PTGS2. (j) Levels of SMAD2 and ZFP36. Two-way ANOVA was performed. Data were presented as mean±standard deviation (SD) of three to five independent experiments. $^{*}P$<0.05 vs. normal, $^{\#}P$<0.05 vs. control, and $^{\&}P$<0.05 vs. hucMSCs-exo$^{\text{mimic NC}}$. Exo-: exosomes; HucMSCs-exo: exosomes secreted by human umbilical cord mesenchymal stem cells; NC: negative control; ANOVA: analysis of variance; CMCs: cardiomyocytes; TUNEL: terminal deoxynucleotidyl transferase dUTP nick end labeling; GPX4: glutathione peroxidase 4; GSH: glutathione; MDA: malondialdehyde; ROS: reactive oxygen species; SLC7A11: solute carrier family 7, member 11; p53: protein 53; PTGS2: prostaglandin G/H synthase 2; SMAD2: mothers against decapentaplegic homolog 2; ZFP36: zinc-finger protein 36; DAPI: 4',6-diamidino-2-phenylindole dihydrochloride; GAPDH: glyceraldehyde-3-phosphate dehydrogenase; prot: protein; FITC: fluorescein isothiocyanate.

which visually revealed that the *let-7a-5p* mimic enabled the inhibition of cell death caused by CVB3. Additionally, *let-7a-5p* was able to counterbalance the redox change induced by CVB3. The levels of GPX4 and GSH were lower in the control group than in the normal group, and the hucMSCs-exo and *let-7a-5p* mimic intervened to normalize them (Figs. 3d and 3e). The MDA and ROS increased after the infection, and the hucMSCs-exo and *let-7a-5p* mimic were capable of bringing down the MDA and ROS levels (Figs. 3f and 3g). Meanwhile, the accumulation of the Fe^{2+} in the control was the highest among all groups, while the hucMSCs-exo and *let-7a-5p* mimic significantly mitigated the boosted ion accumulation (Fig. 3h). The accumulation of Fe^{2+} was lower in the hucMSCs-exo$^{let\text{-}7a\text{-}5p\ mimic}$ group than in the hucMSCs-exo$^{mimic\ NC}$ group. The SLC7A11 levels were higher in the hucMSCs-exo$^{let\text{-}7a\text{-}5p\ mimic}$ group than in the hucMSCs-exo$^{mimic\ NC}$ group. The p53 and PTGS2 expression decreased in the hucMSCs-exo$^{let\text{-}7a\text{-}5p\ mimic}$ group (Fig. 3i). Therefore, in the in vitro model, a series of ferroptosis phenomena occurred in CMCs after the viral infection, and hucMSCs-exo and *let-7a-5p* mimic could inhibit the CVB3-induced ferroptosis. Meanwhile, the effect of hucMSCs-exo$^{let\text{-}7a\text{-}5p\ mimic}$ was better. Moreover, ZFP36 expression increased in the hucMSCs-exo$^{let\text{-}7a\text{-}5p\ mimic}$ group, while SMAD2 decreased (Fig. 3j).

3.5 *Let-7a-5p* targeting E3 ubiquitin ligase SMAD2

Based on our data, the expression of SMAD2, a key regulator of the E3 ubiquitination pathway, was relatively low in normal CMCs. First, the interaction was predicted between *let-7a-5p* and the 3'-untranslated region (3'-UTR) sequence of the *SMAD2* mRNA (Fig. 4a). Then, the interaction between *let-7a-5p* and *SMAD2* was identified by dual-luciferase reporter gene

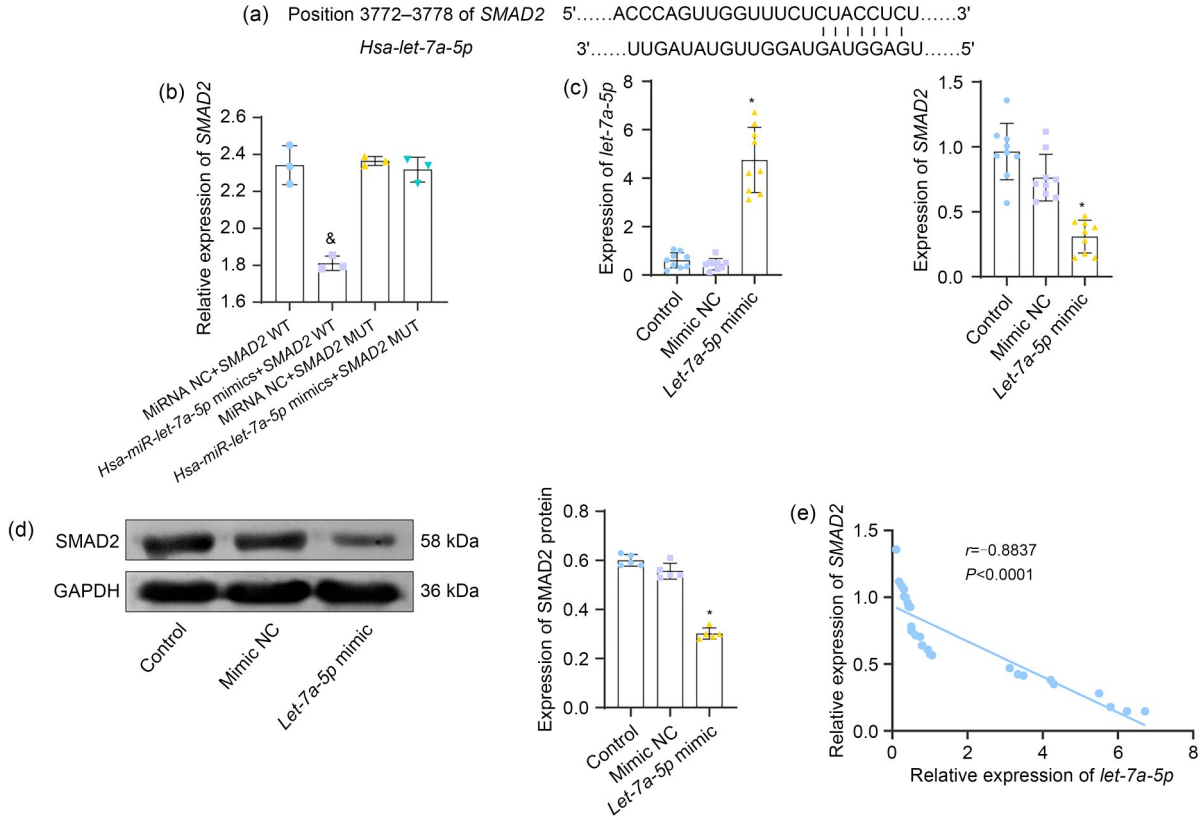

Fig. 4 Interaction between *Let-7a-5p* and SMAD2 to downregulate the expression of SMAD2 in CMCs. (a) Prediction of the interaction between *let-7a-5p* and the mRNA of *SMAD2*. (b) The interaction between *let-7a-5p* and *SMAD2* mRNA was confirmed by dual-luciferase reporter gene assay. (c, d) Levels of *let-7a-5p* and SMAD2. (e) Pearson correlation analysis between the expression of *let-7a-5p* and *SMAD2*. (b–d) Data were presented as mean±standard deviation (SD) of three to nine independent experiments. $^{\&}P<0.05$ vs. mRNA NC+*SMAD2* WT, $^{*}P<0.05$ vs. mimic NC, with one-way ANOVA. SMAD2: mothers against decapentaplegic homolog 2; CMCs: cardiomyocytes; mRNA: messenger RNA; ANOVA: analysis of variance; WT: wild type; MUT: mutant; NC: negative control; GAPDH: glyceraldehyde-3-phosphate dehydrogenase.

assay (Fig. 4b). The *let-7a-5p* mimic inhibited *SMAD2* expression in CVB3-induced CMCs (Figs. 4c and 4d). Correlation analysis showed that *let-7a-5p* was significantly negatively correlated with *SMAD2* (Fig. 4e). Therefore, *let-7a-5p* could target *SMAD2* and downregulate *SMAD2* expression in CMCs.

3.6 *Let-7a-5p* downregulating *SMAD2* to inhibit the ferroptosis of CMCs in vitro

Aiming to further elucidate the functional association of *let-7a-5p* with *SMAD2* as well as the regulatory contribution of CMCs to ferroptosis, we prioritized the quantification of the expression of *let-7a-5p* and *SMAD2* in the in vitro model with the treatment of *let-7a-5p* mimic or oe-*SMAD2* (Fig. 5a). The proliferation changes were observed in different groups (Figs. 5b and 5c). Compared with the mimic NC group, the *let-7a-5p* mimic could facilitate the proliferation of CMCs. Interestingly, even though *SMAD2* was overexpressed, *let-7a-5p* also demonstrated the potency of promoting CMCs proliferation. The results of flow cytometry reflected the inhibitory effects of *let-7a-5p* more clearly (Fig. 5d). When *let-7a-5p* was used, the cell death was considerably inhibited even with overexpressed *SMAD2*. Consistently, the expression of GPX4 and SLC7A11 was promoted in the oe-NC+*let-7a-5p* mimic group, as compared with the oe-NC+mimic NC. The levels of these two proteins were lower in the oe-*SMAD2*+*let-7a-5p* mimic group than in the oe-NC+*let-7a-5p* mimic (Fig. 5e). GSH increased in the treatment of *let-7a-5p* mimic, compared with the mimic NC (Fig. 5f). At the same time, *let-7a-5p* could inhibit the MDA, ROS, and Fe^{2+} levels, and oe-*SMAD2* could alleviate the inhibition of *let-7a-5p* (Figs. 5g–5i).

On the other hand, CVB3-treated CMCs were subjected to ferrostain-1, *let-7a-5p* inhibitor, and si-*SMAD2*. The ferrostain-1 inhibited *SMAD2* mRNA and increased the *let-7a-5p* levels (Figs. S4a and S4b). The cell proliferation increased after ferrostain-1 intervention. si-*SMAD2* could alleviate the effect of *let-7a-5p* inhibitor on cell proliferation (Fig. S4c). Silencing *let-7a-5p* reversed the effects of ferrostain-1 on the promotion of GPX4, SLC7A11, and GSH, as well as the inhibition of MDA, ROS, and Fe^{2+} (Figs. S4d–S4h). However, si-*SMAD2* could alleviate the effect of *let-7a-5p* inhibitor. Based on these findings, it is suggested that *let-7a-5p* can inhibit ferroptosis, at least in part, by directly downregulating *SMAD2*.

3.7 SMAD2/ZFP36 signal axis inhibiting the ferroptosis of CMCs

In order to better understand the role of SMAD2 and ZFP36 in the ferroptosis of CMCs, the interaction was characterized between SMAD2 and ZFP36 via co-immunoprecipitation (co-IP) (Fig. 6a). The si-*SMAD2* or oe-*ZFP36* was transfected into CMCs, and their transfection efficiency was identified (Fig. 6c). In addition, silencing *SMAD2* promoted the expression of *ZFP36*, and the decrease in *SMAD2* also occurred in response to the overexpression of *ZFP36*. As shown in Fig. 6b, the si-*SMAD2*+oe-NC group exhibited increased proliferation in comparison to the si-NC+oe-NC group. In addition, there was an even higher level of cell proliferation observed in the si-*SMAD2*+oe-*ZFP36* group, as compared to the si-*SMAD2*+oe-NC group. The proliferation was markedly promoted after silencing *SMAD2*, and overexpression of *ZFP36* further increased the proliferative activity of CMCs. Besides, the changes in mitochondria, an indicator of ferroptosis, were observed via TEM (Fig. 6d). In the CMCs undergoing ferroptosis, mitochondria shrank in size and mitochondrial cristae became lower in quantity. By contrast, si-*SMAD2* showed inhibitory effects on ferroptosis, thus facilitating the re-shaping of the normal morphology of mitochondria. The GPX4 and GSH in CMCs were also regulated by *SMAD2* and *ZFP36* (Figs. 6e and 6f); the si-*SMAD2* and oe-*ZFP36* increased their levels. The levels of MDA, ROS, and Fe^{2+} decreased in the si-*SMAD2*+oe-NC group compared to the si-NC+oe-NC group. Furthermore, these levels were even lower in the si-*SMAD2*+oe-*ZFP36* group than in the si-*SMAD2*+oe-NC group (Figs. 6g–6i). The overexpression of *ZFP36* also contributed to diminishing the levels of these parameters. Taken together, si-*SMAD2* or oe-*ZFP36* could restore CVB3-induced ferroptosis, indicating that both of these proteins are key regulators of ferroptosis.

3.8 Alleviation of ferroptosis by exo-*let-7a-5p* derived from hucMSCs

The inhibitory regulation of ferroptosis by *let-7a-5p* inspired us to continue the investigation with an in vivo assay. The hucMSCs-exo, hucMSCs-exo$^{\text{inhibitor NC}}$, hucMSCs-exo$^{\textit{let-7a-5p}\text{ inhibitor}}$, hucMSCs-exo$^{\text{mimic NC}}$, and hucMSCs-exo$^{\textit{let-7a-5p}\text{ mimic}}$ were separately injected into VMC mice (Fig. 7a). Firstly, the expression of *let-7a-5p* was identified in exosomes and VMC mice (Figs. 7b

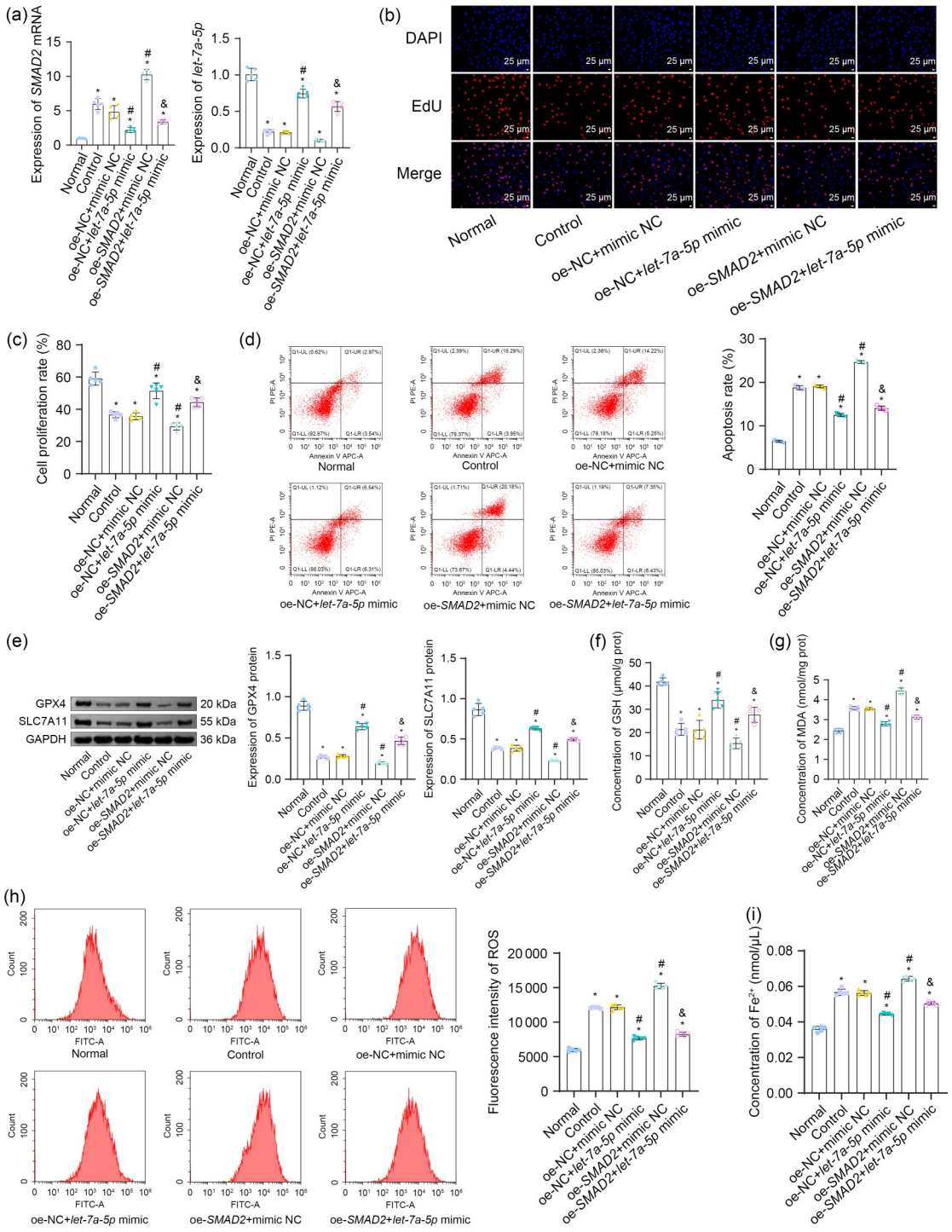

Fig. 5 Inhibited ferroptosis of CMCs via *Let-7a-5p* downregulating *SMAD2*. (a) Expression of *SMAD2* and *let-7a-5p*. (b, c) Proliferation of CMCs detected by EdU assay. (d) Apoptosis rate of CMCs detected by flow cytometry. (e) Protein expression of GXP4 and SLC7A11. (f–i) Levels of GSH, MDA, ROS, and Fe^{2+}. Data were presented as mean±standard deviation (SD) of five independent experiments. $^{*}P$<0.05 vs. normal, $^{\#}P$<0.05 vs. oe-NC+mimic NC, and $^{\&}P$<0.05 vs. oe-*SMAD2*+mimic NC, with one-way ANOVA. SMAD2: mothers against decapentaplegic homolog 2; CMCs: cardiomyocytes; EdU: 5-ethynyl-2'-deoxyuridine; GPX4: glutathione peroxidase 4; SLC7A11: solute carrier family 7, member 11; GSH: glutathione; MDA: malondialdehyde; ROS: reactive oxygen species; ANOVA: analysis of variance; NC: negative control; oe-: overexpression plasmid; DAPI: 4',6-diamidino-2-phenylindole dihydrochloride; GAPDH: glyceraldehyde-3-phosphate dehydrogenase; prot: protein.

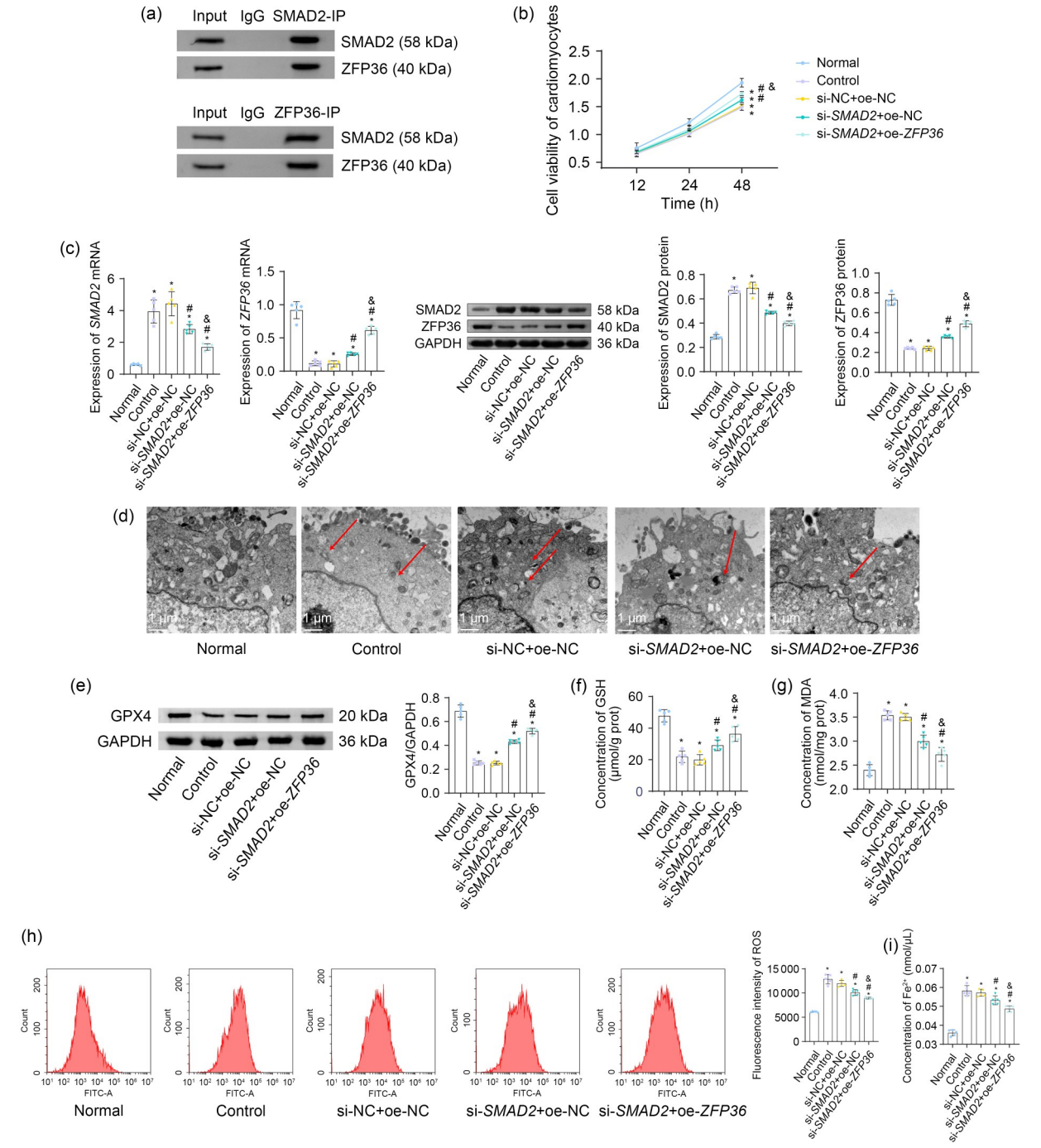

Fig. 6 Inhibited ferroptosis of CMCs by SMAD2/ZFP36 signal axis. (a) Co-IP assays of SMAD2 and ZFP36 in CMCs. (b) After si-*SMAD2* and oe-*ZFP36* intervention, the proliferation activity of CMCs was analyzed. Two-way ANOVA was performed. (c) The mRNA expression and protein levels of SMAD2 and ZFP36. (d) The morphology and structure of mitochondria from CMCs under TEM. The red arrows indicate the reduced volume of mitochondria in CMCs and the decreased number of cristae. (e) Expression of GXP4. (f–i) Levels of GSH, MDA, ROS, and Fe^{2+}. One-way ANOVA was performed. Data were presented as mean±standard deviation (SD) of five independent experiments. $^{*}P$<0.05 vs. normal, $^{\#}P$<0.05 vs. si-NC+oe-NC, and $^{\&}P$<0.05 vs. si-SMAD2+oe-NC. SMAD2: mothers against decapentaplegic homolog 2; ZFP36: zinc-finger protein 36; CMCs: cardiomyocytes; Co-IP: co-immunoprecipitation; ANOVA: analysis of variance; TEM: transmission electron microscopy; GPX4: glutathione peroxidase 4; GSH: glutathione; MDA: malondialdehyde; ROS: reactive oxygen species; NC: negative control; IgG: immunoglobulin G; si-: small interfering RNA; oe-: overexpression plasmid; GAPDH: glyceraldehyde-3-phosphate dehydrogenase; FITC: fluorescein isothiocyanate; prot: protein.

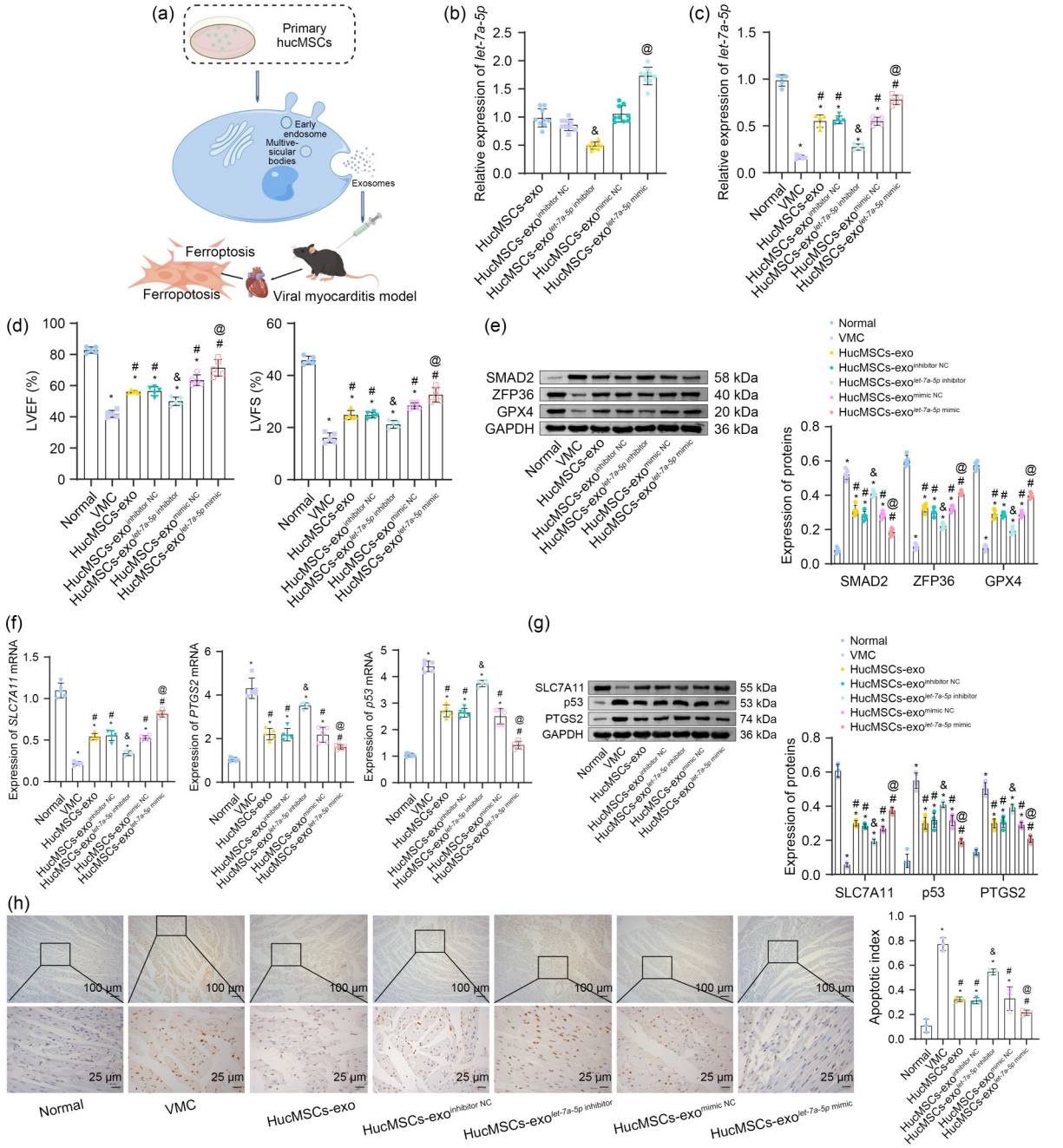

Fig. 7 Therapeutic effects of exo-*let-7a-5p* derived from hucMSCs on ferroptosis in vivo. (a) Diagram of hucMSCs-exo intervention in VMC mice. (b) Expression level of *let-7a-5p* in exosomes. (c) Expression level of *let-7a-5p* in VMC mice. (d) Levels of LVEF and LVFS. One-way ANOVA was performed. (e) Protein expression of SMAD2, ZFP36, and GXP4 in VMC mice. Two-way ANOVA was performed. (f, g) The mRNA and protein expression of SLC7A11, PTGS2, and p53. One-way ANOVA and two-way ANOVA were performed. (h) Apoptosis rate using TUNEL assay. One-way ANOVA was performed. Data were presented as mean±standard deviation (SD) of three to nine independent experiments. $^{*}P$<0.05 vs. normal, $^{\#}P$<0.05 vs. VMC, $^{\&}P$<0.05 vs. hucMSCs-exo$^{\text{inhibitor NC}}$, and $^{@}P$<0.05 vs. hucMSCs-exo$^{\text{mimic NC}}$. Exo: exosomes; HucMSCs: human umbilical cord mesenchymal stem cells; VMC: viral myocarditis; LVEF: left ventricular ejection fraction; LVFS: left ventricular fractional shortening; SMAD2: mothers against decapentaplegic homolog 2; ZFP36: zinc-finger protein 36; GPX4: glutathione peroxidase 4; ANOVA: analysis of variance; mRNA: messenger RNA; SLC7A11: solute carrier family 7, member 11; p53: protein 53; PTGS2: prostaglandin G/H synthase 2; TUNEL: terminal deoxynucleotidyl transferase dUTP nick end labeling; NC: negative control; GAPDH: glyceraldehyde-3-phosphate dehydrogenase.

and 7c). The results showed that the treatment with hucMSCs-exo increased the expression of *let-7a-5p*. Compared with the hucMSCs-exo$^{\text{inhibitor NC}}$ group, the *let-7a-5p* level was reduced in the hucMSCs-exo$^{\textit{let-7a-5p}\text{ inhibitor}}$ group, and was higher in the hucMSCs-exo$^{\textit{let-7a-5p}\text{ mimic}}$ group than in the hucMSCs-exo$^{\text{mimic NC}}$ group. To examine the recovery of function in VMC models, the LVEF and LVFS of mice with different treatments were measured (Fig. 7d). The values of these two parameters were extremely low in the VMC group, implying defects in heart functions. When subjected to hucMSCs-exo treatment, either LVEF or LVFS had a noticeable rise, which was a sign of the recovery of heart functions. Next, the expression of SMAD2 and ZFP36 was analyzed in mice (Fig. 7e). SMAD2 expression increased in VMC mice, while ZFP36 expression decreased. The internalization of *let-7a-5p* favored the ZFP36 expression but suppressed the SMAD2 in VMC mice. The ZFP36 protein level was also upregulated in the hucMSCs-exo$^{\textit{let-7a-5p}\text{ mimic}}$ group, and the SMAD2 level decreased. In agreement with the in vitro assay, GPX4 in VMC mice was predominantly downregulated, but the hucMSCs-exo$^{\textit{let-7a-5p}\text{ mimic}}$ was capable of eliciting a restoration of GPX4 back to the original level (Fig. 7e). The expression of PTGS2 and p53 decreased in the hucMSCs-exo$^{\textit{let-7a-5p}\text{ mimic}}$ group compared with the hucMSCs-exo$^{\text{mimic NC}}$ group, while that of SLC7A11 increased (Figs. 7f and 7g). By analyzing the expression of ferroptosis-related proteins, including SLC7A11, PTGS2, and p53, the inhibitory effect of *let-7a-5p* on ferroptosis was confirmed again. The apoptosis of myocardial tissues of different groups was determined using TUNEL assay (Fig. 7h). It was found that the hucMSCs-exo$^{\textit{let-7a-5p}\text{ mimic}}$ could reduce the apoptosis rate. Accordingly, the exosomes enriched with *let-7a-5p* could mediate the downregulation of *SMAD2* to promote *ZFP36*, providing therapeutic potency to rescue CVB3-induced VMC in mice.

4 Discussion

In this study, we have identified a strong connection between VMC and ferroptosis through the examination of ferroptosis-related biomarkers. Ferroptosis is a recently characterized type of programmed cell death, which has been closely associated with the development of inflammation (Sun et al., 2020). As a result, the aberrant regulation of ferroptosis may lead to a myriad of inflammation-related diseases. Importantly, changes in the levels of signature biomarkers can be utilized to assess the development of ferroptosis (Chen X et al., 2021). Moreover, due to relevant changes in the redox status, ferroptosis development can be reflected by changes in the levels of GSH, GXP4, and ROS (Jiang et al., 2021). In this study, we monitored the development of ferroptosis in both CMCs and VMC mice by detecting the changes in these biomarkers.

Exosomes isolated from hucMSCs can affect the development of diseases (Hu et al., 2020; Dong et al., 2021). Our study found that, after the intervention involving hucMSCs-exo, the proliferation activity of VMC cells improved and the cell death rate decreased. Furthermore, the levels of ferroptosis-related indicators changed. Those of GPX4, GSH, and SLC7A11 increased, while MDA, ROS, and Fe^{2+} decreased. These findings suggested that CVB3-induced CMC ferroptosis was suppressed by hucMSCs-exo, which could alleviate cell damage caused by infection with CVB3. As a molecular delivery medium, exosomes can participate in cellular biological processes by transporting subsets of proteins, lipids, and nucleic acids (el Andaloussi et al., 2013), exhibiting the advantages of drug delivery tools. Their natural targeting properties and wide biodistribution provide them increased utility as drug delivery systems in preclinical settings (Murphy et al., 2019). In fact, exosomes have been widely concerned as a new therapeutic strategy and carriers of pharmaceutical products (Silva et al., 2021; Velot et al., 2021; Zhu et al., 2022). Engineered exosomes encapsulate nanoparticles containing enzymes or drugs and act on target cells with efficient penetration and targeting capabilities, thereby promoting the treatment of diseases (Liu C et al., 2022; Wu et al., 2022). Thus, we hypothesized that hucMScs-derived exosomes may have contents that alleviate cell damage.

Based on recent advances in cell delivery and other technologies, RNA therapies such as mRNA, circular RNA (circRNA), and microRNA (miRNA) have shown great potential (Garbo et al., 2022; Li MY et al., 2022; Liu X et al., 2022). Specifically, miRNA therapy involves the regulation of miRNA levels to enhance or block its functionality (Krützfeldt et al., 2005; Garbo et al., 2022). Studies have highlighted that miRNAs enriched in exosomes can affect the development of diseases by regulating the expression

of downstream genes, including atherosclerosis (Zhu et al., 2019), depression (Li et al., 2020), acute liver injury (Shao et al., 2020), and breast cancer (Chen B et al., 2021). In our study, *let-7a-5p* was enriched in exosomes derived from hucMSCs, consistent with previous studies (Li KL et al., 2022). When using a *let-7a-5p* mimic to treat the CVB3-induced cells, we observed further enhancement of the proliferative activity of CMCs. The levels of GSH, GXP4, and SLC7A11 were suppressed during ferroptosis but were remarkably elevated with the internalization of *let-7a-5p*. In comparison, the levels of ferroptosis-associated biomarkers declined significantly, including ROS, MDA, and Fe^{2+}. Therefore, we speculated that exo-*let-7a-5p* derived from hucMSCs could inhibit CVB3-induced ferroptosis.

SMAD2, as one of the key regulators of the SMAD signaling pathway, has been implicated in the regulation of ferroptosis (Liu et al., 2021). The expression of ZFP36, a key regulator to inhibit ferroptosis, was much lower in platinum-sensitive cells associated with ferroptosis than in platinum-resistant cells (Li XX et al., 2021). This is similar to our findings, that is, *SMAD2* expression was elevated and *ZFP36* expression decreased in ferroptosis-associated VMC. Moreover, our data showed that *SMAD2* interacted with *ZFP36* and that inhibiting *SMAD2* could upregulate the expression of *ZFP36*. Overexpression of *ZFP36* could reduce the level of *SMAD2*. Simultaneous treatment of silencing *SMAD2* and overexpressing *ZFP36* further suppressed ferroptosis in VMC cells. Through further analysis, we confirmed that *let-7a-5p* targeted *SMAD2* mRNA and inhibited *SMAD2* expression, ultimately leading to the inhibition of ferroptosis. In our established VMC model, the effects of *SMAD2* overexpression on ferroptosis development were largely reversed by the internalization of *let-7a-5p*. This suggested that *let-7a-5p*, which is enriched in exosomes, has the potential to alleviate CVB3-induced ferroptosis by regulating *SMAD2* signaling.

Studies have established a correlation between *let-7a-5p* and pulmonary fibrosis (Thakur et al., 2022) and its ability to regulate the innate immune response (Ueta et al., 2023). *Let-7a-5p* delivered by exosomes was shown to be involved in the activation of M1 macrophages (Yan et al., 2021). These observations suggest that *let-7a-5p* may also have a regulatory impact on other cells besides CMCs. However, due to the time constraints, it remains to be further explored whether or not hucMSC exo-*let-7a-5p* affects other biological processes in CVB3-induced VMC, such as those in cardiac fibroblasts and immune cells. It is also important to note that the successful uptake of exosomes by the heart in VMC mice requires further confirmation, given the limitations of our experimental conditions. We further plan to investigate other miRNAs targeting *SMAD2*. Additionally, one of the potential therapeutic strategies to alleviate VMC is to increase *let-7a-5p*, although this may not be the optimal choice; the regulatory mechanism of organisms is complex, and further research is necessary for a better understanding.

5 Conclusions

In this study, we demonstrated that ferroptosis is involved in the development of CVB3-induced VMC, which can be alleviated by hucMSCs-derived exosomes via delivering their *let-7a-5p* to regulate SMAD2 signaling in CMCs. This finding might provide potential strategies for the treatment of VMC.

Data availability statement

The dataset used or analyzed during the current study is available from the corresponding author on reasonable request.

Acknowledgments

This work was supported by the China Postdoctoral Science Foundation (No. 2022M712252) and the Natural Science Foundation of Sichuan Province, China (No. 2023NSFSC1634).

Author contributions

Xin LI made significant contributions to conceptualization, data curation, investigation, methodology, validation, and writing of the original draft. Yanan HU, Yueting WU, Zuocheng YANG, and Yang LIU contributed to conceptualization, formal analysis, investigation, software, validation, and writing of the original draft. Hanmin LIU contributed significantly to conceptualization, funding acquisition, project administration, supervision, and review. All authors have read and approved the final version, and therefore, have full access to all the data in the study and take responsibility for the integrity and security of the data.

Compliance with ethics guidelines

Xin LI, Yanan HU, Yueting WU, Zuocheng YANG, Yang LIU, and Hanmin LIU declare that they have no conflict of interest.

The entire operation and experiments related to animals were approved by the Animal Ethics Committee of West China

Second University Hospital, Sichuan University, Chengdu, China (No. 2022-137). All institutional and national guidelines for the care and use of laboratory animals were followed.

References

Bao MH, Feng X, Zhang YW, et al., 2013. Let-7 in cardiovascular diseases, heart development and cardiovascular differentiation from stem cells. *Int J Mol Sci*, 14(11):23086-23102. https://doi.org/10.3390/ijms141123086

Camaschella C, Nai A, Silvestri L, 2020. Iron metabolism and iron disorders revisited in the hepcidin era. *Haematologica*, 105(2):260-272. https://doi.org/10.3324/haematol.2019.232124

Chen B, Sang YT, Song XJ, et al., 2021. Exosomal miR-500a-5p derived from cancer-associated fibroblasts promotes breast cancer cell proliferation and metastasis through targeting USP28. *Theranostics*, 11(8):3932-3947. https://doi.org/10.7150/thno.53412

Chen CY, Choong OK, Liu LW, et al., 2019. MicroRNA let-7-TGFBR3 signalling regulates cardiomyocyte apoptosis after infarction. *EBioMedicine*, 46:236-247. https://doi.org/10.1016/j.ebiom.2019.08.001

Chen P, Xie YQ, Shen E, et al., 2011. Astragaloside IV attenuates myocardial fibrosis by inhibiting TGF-β1 signaling in coxsackievirus B3-induced cardiomyopathy. *Eur J Pharmacol*, 658(2-3):168-174. https://doi.org/10.1016/j.ejphar.2011.02.040

Chen X, Comish PB, Tang DL, et al., 2021. Characteristics and biomarkers of ferroptosis. *Front Cell Dev Biol*, 9:637162. https://doi.org/10.3389/fcell.2021.637162

Dong LY, Wang Y, Zheng TT, et al., 2021. Hypoxic hUCMSC-derived extracellular vesicles attenuate allergic airway inflammation and airway remodeling in chronic asthma mice. *Stem Cell Res Ther*, 12:4. https://doi.org/10.1186/s13287-020-02072-0

el Andaloussi S, Mäger I, Breakefield XO, et al., 2013. Extracellular vesicles: biology and emerging therapeutic opportunities. *Nat Rev Drug Discov*, 12(5):347-357. https://doi.org/10.1038/nrd3978

Garbo S, Maione R, Tripodi M, et al., 2022. Next RNA therapeutics: the mine of non-coding. *Int J Mol Sci*, 23(13):7471. https://doi.org/10.3390/ijms23137471

Gu XH, Li YC, Chen KX, et al., 2020. Exosomes derived from umbilical cord mesenchymal stem cells alleviate viral myocarditis through activating AMPK/mTOR-mediated autophagy flux pathway. *J Cell Mol Med*, 24(13):7515-7530. https://doi.org/10.1111/jcmm.15378

Hu Y, Zhang Y, Ni CY, et al., 2020. Human umbilical cord mesenchymal stromal cells-derived extracellular vesicles exert potent bone protective effects by CLEC11A-mediated regulation of bone metabolism. *Theranostics*, 10(5):2293-2308. https://doi.org/10.7150/thno.39238

Huber SA, 2016. Viral myocarditis and dilated cardiomyopathy: etiology and pathogenesis. *Curr Pharm Des*, 22(4):408-426. https://doi.org/10.2174/1381612822666151222160500

Inamdar AA, Inamdar AC, 2016. Heart failure: diagnosis, management and utilization. *J Clin Med*, 5(7):62. https://doi.org/10.3390/jcm5070062

Jiang XJ, Stockwell BR, Conrad M, 2021. Ferroptosis: mechanisms, biology and role in disease. *Nat Rev Mol Cell Biol*, 22(4):266-282. https://doi.org/10.1038/s41580-020-00324-8

Krützfeldt J, Rajewsky N, Braich R, et al., 2005. Silencing of microRNAs *in vivo* with 'antagomirs'. *Nature*, 438(7068):685-689. https://doi.org/10.1038/nature04303

Li DP, Wang Y, Jin XR, et al., 2020. NK cell-derived exosomes carry miR-207 and alleviate depression-like symptoms in mice. *J Neuroinflammation*, 17:126. https://doi.org/10.1186/s12974-020-01787-4

Li J, Xie YW, Li LW, et al., 2021. MicroRNA-30a modulates type I interferon responses to facilitate coxsackievirus B3 replication *via* targeting tripartite motif protein 25. *Front Immunol*, 11:603437. https://doi.org/10.3389/fimmu.2020.603437

Li JH, Tu JH, Gao H, et al., 2021. MicroRNA-425-3p inhibits myocardial inflammation and cardiomyocyte apoptosis in mice with viral myocarditis through targeting TGF-β1. *Immun Inflamm Dis*, 9(1):288-298. https://doi.org/10.1002/iid3.392

Li KL, Yan GH, Huang HJ, et al., 2022. Anti-inflammatory and immunomodulatory effects of the extracellular vesicles derived from human umbilical cord mesenchymal stem cells on osteoarthritis via M2 macrophages. *J Nanobiotechnol*, 20:38. https://doi.org/10.1186/s12951-021-01236-1

Li MY, Li Y, Li SQ, et al., 2022. The nano delivery systems and applications of mRNA. *Eur J Med Chem*, 227:113910. https://doi.org/10.1016/j.ejmech.2021.113910

Li XX, Xiong L, Wen Y, et al., 2021. Comprehensive analysis of the tumor microenvironment and ferroptosis-related genes predict prognosis with ovarian cancer. *Front Genet*, 12:774400. https://doi.org/10.3389/fgene.2021.774400

Liu C, Yan XJ, Zhang YJ, et al., 2022. Oral administration of turmeric-derived exosome-like nanovesicles with anti-inflammatory and pro-resolving bioactions for murine colitis therapy. *J Nanobiotechnol*, 20:206. https://doi.org/10.1186/s12951-022-01421-w

Liu G, Ma JY, Hu G, et al., 2021. Identification and validation of a novel ferroptosis-related gene model for predicting the prognosis of gastric cancer patients. *PLoS ONE*, 16(7):e0254368. https://doi.org/10.1371/journal.pone.0254368

Liu X, Zhang Y, Zhou SR, et al., 2022. Circular RNA: an emerging frontier in RNA therapeutic targets, RNA therapeutics, and mRNA vaccines. *J Control Release*, 348:84-94. https://doi.org/10.1016/j.jconrel.2022.05.043

Mathieu M, Martin-Jaular L, Lavieu G, et al., 2019. Specificities of secretion and uptake of exosomes and other extracellular vesicles for cell-to-cell communication. *Nat Cell Biol*, 21(1):9-17.

https://doi.org/10.1038/s41556-018-0250-9

Murphy DE, de Jong OG, Brouwer M, et al., 2019. Extracellular vesicle-based therapeutics: natural versus engineered targeting and trafficking. *Exp Mol Med*, 51(3):1-12. https://doi.org/10.1038/s12276-019-0223-5

Qiao C, Xu W, Zhu W, et al., 2008. Human mesenchymal stem cells isolated from the umbilical cord. *Cell Biol Int*, 32(1):8-15. https://doi.org/10.1016/j.cellbi.2007.08.002

Rodríguez-Graciani KM, Chapa-Dubocq XR, Ayala-Arroyo EJ, et al., 2022. Effects of ferroptosis on the metabolome in cardiac cells: the role of glutaminolysis. *Antioxidants (Basel)*, 11(2):278. https://doi.org/10.3390/antiox11020278

Shao MY, Xu Q, Wu ZR, et al., 2020. Exosomes derived from human umbilical cord mesenchymal stem cells ameliorate IL-6-induced acute liver injury through miR-455-3p. *Stem Cell Res Ther*, 11:37. https://doi.org/10.1186/s13287-020-1550-0

Silva AKA, Morille M, Piffoux M, et al., 2021. Development of extracellular vesicle-based medicinal products: a position paper of the group "Extracellular Vesicle translatiOn to clinicaL perspectiVEs – EVOLVE France". *Adv Drug Deliv Rev*, 179:114001. https://doi.org/10.1016/j.addr.2021.114001

Sun LF, Zhu M, Feng W, et al., 2019. Exosomal miRNA let-7 from menstrual blood-derived endometrial stem cells alleviates pulmonary fibrosis through regulating mitochondrial DNA damage. *Oxid Med Cell Longev*, 2019:4506303. https://doi.org/10.1155/2019/4506303

Sun YT, Chen P, Zhai BT, et al., 2020. The emerging role of ferroptosis in inflammation. *Biomed Pharmacother*, 127:110108. https://doi.org/10.1016/j.biopha.2020.110108

Thakur D, Taliaferro O, Atkinson M, et al., 2022. Inhibition of nuclear factor κB in the lungs protect bleomycin-induced lung fibrosis in mice. *Mol Biol Rep*, 49(5):3481-3490. https://doi.org/10.1007/s11033-022-07185-8

Ueta M, Nishigaki H, Komai S, et al., 2023. Positive regulation of innate immune response by miRNA-let-7a-5p. *Front Genet*, 13:1025539. https://doi.org/10.3389/fgene.2022.1025539

Velot É, Madry H, Venkatesan JK, et al., 2021. Is extracellular vesicle-based therapy the next answer for cartilage regeneration? *Front Bioeng Biotechnol*, 9:645039. https://doi.org/10.3389/fbioe.2021.645039

Wang GY, Yuan JT, Cai X, et al., 2020. HucMSC-exosomes carrying miR-326 inhibit neddylation to relieve inflammatory bowel disease in mice. *Clin Transl Med*, 10(2):e113. https://doi.org/10.1002/ctm2.113

Wu TT, Liu Y, Cao Y, et al., 2022. Engineering macrophage exosome disguised biodegradable nanoplatform for enhanced sonodynamic therapy of glioblastoma. *Adv Mater*, 34(15):2110364. https://doi.org/10.1002/adma.202110364

Xia YZ, Shan GF, Yang H, et al., 2021. Cisatracurium regulates the CXCR4/let-7a-5p axis to inhibit colorectal cancer progression by suppressing TGF-β/SMAD2/3 signalling. *Chem Biol Interact*, 339:109424. https://doi.org/10.1016/J.CBI.2021.109424

Yan C, Zhou QY, Wu J, et al., 2021. Csi-let-7a-5p delivered by extracellular vesicles from a liver fluke activates M1-like macrophages and exacerbates biliary injuries. *Proc Natl Acad Sci USA*, 118(46):e2102206118. https://doi.org/10.1073/pnas.2102206118

Yuan XQ, Li TF, Shi L, et al., 2021. Human umbilical cord mesenchymal stem cells deliver exogenous miR-26a-5p via exosomes to inhibit nucleus pulposus cell pyroptosis through METTL14/NLRP3. *Mol Med*, 27:91. https://doi.org/10.1186/s10020-021-00355-7

Zhu DS, Liu S, Huang K, et al., 2022. Intrapericardial exosome therapy dampens cardiac injury via activating Foxo3. *Circ Res*, 131(10):e135-e150. https://doi.org/10.1161/circresaha.122.321384

Zhu JM, Liu B, Wang ZY, et al., 2019. Exosomes from nicotine-stimulated macrophages accelerate atherosclerosis through miR-21-3p/PTEN-mediated VSMC migration and proliferation. *Theranostics*, 9(23):6901-6919. https://doi.org/10.7150/thno.37357

Supplementary information

Materials and methods; Figs. S1–S4